https://doi.org/10.48048/tis.2024.7807

Anticancer Identification and Molecular Docking of Cowanol from *Garcinia fusca* Against Histone Deacetylase Domains

Sakdiphong Punpai[1], Audchara Saenkham[2], Pornthip Boonsri[2], Kiattawee Choowongkomon[3], Sunit Suksamrarn[2] and Wanlaya Tanechpongtamb[4,*]

[1]Innovative Learning Center (ILC), Srinakharinwirot University, Bangkok 10110, Thailand
[2]Department of Chemistry and Center of Excellence for Innovation in Chemistry, Faculty of Science, Srinakharinwirot University, Bangkok 10110, Thailand
[3]Department of Biochemistry, Faculty of Science, Kasetsart University, Bangkok 10903, Thailand
[4]Department of Biochemistry, Faculty of Medicine, Srinakharinwirot University, Bangkok 10110, Thailand

([*]Corresponding author's e-mail: wanlaya@g.swu.ac.th)

Received: 4 December 2023, Revised: 8 January 2024, Accepted: 15 January 2024, Published: 25 June 2024

Abstract

The inhibition of HDAC activity is presently one of the main targets for anticancer drug development. This study aimed to investigate the anticancer effect of cowanol *via* inhibition of HDAC and apoptosis induction in leukemic Jurkat cells. Computational analysis and HDAC inhibitor screening assays were used to determine the properties of cowanol as an HDAC inhibitor in Jurkat cells. MTT assays and Hoechst staining were performed to observe the cytotoxicity and apoptotic induction effect of cowanol. *In silico* docking analysis revealed that cowanol could tightly bind to the active sites of both HDAC class I (HDAC 2 and 8) and HDAC class II (HDAC 4 and 7) with a similar mode of binding to the reference inhibitors. Importantly, cowanol obviously interacts with the zinc ion at the catalytic center as well as with other amino acid residues in the active region, indicating its possible function as an HDAC inhibitor. The ADME results showed that cowanol possessed acceptable pharmacokinetics and drug-likeness properties, which suggested oral bioavailability. In addition, the screening assay demonstrated that cowanol could inhibit HDAC at 20 - 60 % compared to the standard HDAC inhibitor, SAHA. Moreover, the cytotoxic effect of cowanol against Jurkat cells with the IC_{50} was 18.19 ± 0.44 μM. For the mode of cell death, nuclear condensation and apoptotic bodies were characterized, supporting the role of the apoptosis inducer cowanol. Hence, our results indicated a potential new role of cowanol as an HDAC inhibitor. The cytotoxic mode of cowanol was illustrated as apoptotic inducer, which is a well-known target for anticancer drug development.

Keywords: ADME, Cowanol, *Garcinia fusca*, Histone deacetylase inhibitor, *In silico* docking, Leukemia

Introduction

The alteration of epigenetics is indicated as one crucial factor for cancer development, especially the changes in the posttranslational modification of histones with acetylation and deacetylation. This process is normally controlled by opposing actions of 2 large families of enzymes, including histone acetyltransferases (HATs) and histone deacetylases (HDACs) [1]. HATs mediate hyperacetylation of the histone tail at the N-terminus, which results in an open form of chromatin and gene activation, while HDACs act in the opposite way in which a closed structure of chromatin is formed and gene expression is inhibited. An imbalance of these 2 groups of enzymes is not surprisingly associated with cancer initiation and progression [2]. This is supported by numerous studies showing that oncogene and tumor suppressor gene aberrations are related to higher levels of HDAC gene expression in a variety of human cancer cells [3,4]. Thus, inhibiting HDACs is one promising method for cancer treatment.

HDACs are divided into 4 classes according to their sequence homology to yeast. Class I is composed of HDACs 1, 2, 3 and 8. Class II is subdivided into IIa (HDACs 4, 5, 6, 7 and 9) and IIb (HDACs 6 and 10). Class III consists of sirtuins 1 - 7 and class IV comprises only HDAC 11. Class I, II, and IV HDACs have Zn^{2+} in the catalytic pocket sites, whereas class III HDACs require nicotinamide adenine dinucleotide (NAD^{+}) as a cofactor [5]. Overexpression of HDACs, particularly class I and II HDACs, is associated with tumorigenesis in several cancer types, such as breast, ovarian, liver, lung, cervical, and colorectal cancers [6-9]. In recent years, many compounds that could inhibit the activity of HDACs or HDAC inhibitors

(HDACis) have been discovered as effective anticancer drugs by promoting cell cycle arrest, cell differentiation, or cell apoptosis. Several HDACis have already been approved by the US Food and Drug Administration (FDA), including vorinostat, romidepsin, panobinostat, and belinostat [10]. Although an increasing number of HDACis have been characterized, there has been considerable effort to develop HDACis, especially from nontoxic natural resources.

Garcinia plants are recognized as a rich source of natural xanthones, a group of compounds that provides a wide range of biological effects, such as anticancer, antibacterial, antioxidant, and antiviral effects [11-17]. Young leaves of *G. fusca* can be eaten or cooked in curry, while stems, roots, and leaves are traditionally used for the treatment of coughs and indigestion, relief of fever, and improvement of blood circulation. From these potential uses in medicine, several active compounds including geranylated xanthones have been extracted from *G. fusca* and tested for their medicinal purposes [18,19]. Our previous studies have reported that the xanthone cowaxanthone, extracted from *G. fusca*, exhibited apoptosis-inducing activity in leukemic T cells through HDAC inhibition [20]. Additionally, our recent work discovered the anticancer effect of cowanin, a major xanthone member extracted from the stem barks of *G. fusca*, on leukemic T cells (Jurkat cells). The mechanism occurred through inducing apoptosis and autophagy via the PI3K/AKT/mTOR pathway and HDAC inhibition [19]. Cowanol is also one of the major geranylated xanthones isolated from the stem barks of *G. fusca* (**Figure 1**). Previous data revealed that cowanol has various pharmacological effects, including antimicrobial, antimalarial, anticholinesterase [18], and anticancer effects [21]. Regarding the anticancer effect, cowanol has demonstrated cytotoxic activity against lung (NC1-H187), breast (MCF-7), and colon cancer cell lines (DLD-1) [22,23]. However, the role of HDAC and the underlying mechanism of the effect of cowanol have not yet been investigated.

Thus, we aimed to evaluate the role of cowanol as an HDACi and the sequential mechanism of apoptosis induction. The screening of HDAC inhibition activity was performed by computational *in silico* docking followed by the *in vitro* HDAC inhibition assay. The cytotoxicity and mode of cell death, apoptosis, was evaluated by observing nuclear morphology and caspase-3 activation.

Materials and methods

Reagents

Human leukemic T cells (Jurkat cells), A549 human lung carcinoma, PC-3 human prostatic carcinoma cells, and Vero cells were acquired from the American Type Culture Collection and purchased from American Type Culture Collection (ATCC, USA). RPMI 1640 (Roswell Park Memorial Institute) medium, fetal bovine serum (FBS), and penicillin–streptomycin were obtained from Gibco (Invitrogen, USA). 3-(4,5-Dimethylthiazol-2-yl)-2,5 diphenyltetrazolium bromide (MTT) was obtained from USB Corporation, USA. The Histone Deacetylase Assay Kit (CS1010) was purchased from Sigma–Aldrich, USA. Hoechst 33342 fluorescent solution (H3570) was obtained from Invitrogen, USA.

Plant materials

Stem barks of *G. fusga* were air-dried and collected from Yangtalad District, Kalasin Province, Thailand, in January 2016. The Laboratory of Natural Product Research Unit, Department of Chemistry, Faculty of Science, Srinakharinwirot University, Thailand, has received a voucher specimen of AS 001.

Extraction and isolation

The dry-ground barks of *G. fusca* (10 kg) were thoroughly extracted with EtOAc at room temperature. The solvent was then evaporated to produce an EtOAc extract (271 g of brown residue). Chromatographic separation on silica gel (eluting with a gradient of *n*-hexane-acetone, 96:4 to 0:100, v/v) and acetone-MeOH (95:5 - 0:100, v/v) of the obtained EtOAc soluble extract provided 13major fractions (E1 to E13) according to their TLC observations. Further column chromatography (CC) (eluting with *n*-hexane-acetone (96:5 to 0:100, v/v) of the E11-fraction (29 g) followed by 3 successive CC with *n*-hexane–acetone, cowanol (2 g) was yielded as a yellow solid. The chemical structure of cowanol was evident by its NMR spectroscopic data analysis.

Cell culture

Jurkat leukemic T cells, A549 human lung cancer cells, PC-3 human prostatic carcinoma cells, and Vero cells were obtained from the American Type Culture Collection (ATCC; Manassas, VA, USA). Jurkat cells were cultivated in RPMI 1640, while A549, PC-3 and Vero cells were grown in DMEM (Gibco, Waltham, MA, USA) containing 10 % fetal bovine serum (FBS), 100 units/mL penicillin and 100 µg/mL

streptomycin (Gibco, Waltham, MA, USA). These cells were all grown in a humidified environment with 5 % CO_2 and 37 °C.

***In silico* docking study**

To understand the selective inhibitory effect of cowanol for each HDAC class and isoform, we performed docking of cowanol into the active sites of human HDAC class I (HDAC 2 and 8) and HDAC class II (HDAC 4 and 7) using the GOLD 5.3.0 program [19]. The RCSB Protein Data Bank was used to retrieve the 3-dimensional (3D) crystal structure of human HDAC 2, 4, 7 and 8 enzymes (PDB codes: 3MAX [24], 2VQM [19], 3C10 [25] and 1T64 [26], respectively). The binding of cowanol was further evaluated using reference HDAC inhibitors, which comprised trichostatin A (TSA), suberoylanilide hydroxamic acid (SAHA) and Belinostat (PXD-101). The chemical structures of all ligands were found in the PubChem compound database (http://pubchem.ncbi.nlm.nih.gov/compound). The CHEMPLP parameter was used for docking, and accuracy testing of the overlays was determined by calculating the root mean square deviation (RMSD) below 2 Å and was submitted to 100 cycles before analysis. Drug BIOVIA Discovery Studio 2016 software (DS, version 2016, BIOVIA Corporate Europe, Cambridge, UK) was used to optimize the individual HDAC coordination of the target proteins and the cowano1 molecule, and the UCSF Chimera program was used to represent the molecule-HDAC interaction [27].

ADME predictions

The ADME study (standing for Absorption, Distribution, Metabolism, and Elimination) was conducted using the web-based application SwissADME software (www.swissadme.ch/) of the Swiss Institute of Bioinformatics (http://www.sib.swiss) [28]. This free online software allows physiochemical predictions using Lipinski's rule of 5 for the phytochemical characteristics of cowanol, including its molecular weight, hydrogen bond donor and hydrogen bond acceptor, number of rotatable bonds, polar surface area, and molinspiration Log. It also allows for the calculation of Drug-likeness, which is an essential role in the discovery of new drugs and development [29]. Herein, such properties of the potential compounds were calculated in comparisons with pre-clinical (TSA) and clinical drugs HDACi (SAHA and Belinostat).

HDAC inhibitor screening assay

HDAC inhibitor activity was screened in accordance with the kit's manufacturer-supplied procedure (Sigma-Aldrich, MO, USA). In summary, Jurkat nuclear extract, which served as an HDAC source, was combined with cowanol. Then, a substrate with a fluorescent group was added after the sample reactions. Using a Synergy TM HT Multi-Mode Microplate Reader (Bio-Tek Instrument, USA) with an excitation wavelength of 360 nm and an emission wavelength of 460 nm, the fluorescence product was monitored after 10 min of incubation. As a positive control (SAHA), a well-known and strong hydroxamic acid-based HDAC inhibitor was applied.

Cell proliferation assay

Jurkat, A549, PC-3, and Vero cells were plated at a density of 1 - 5×10^4 cells/well in 96-well plates. These cells were then exposed to several concentrations of cowanol (0, 1.25, 2.5, 5, 10, 20, 40, 80 and 100 μM) for 24, 48 and 72 h, respectively. The medium was then removed, and MTT solution (final concentration of 0.5 mg/mL) was added, followed by a 2 h incubation period at 37 °C. The colorimetric intensity of MTT was quantified by using a microplate reader (Bio-Tek Instruments, USA) to measure a wavelength of 570 nm. The inhibitory concentration at 50 % (IC_{50}) was calculated.

Determination of nuclear condensation

Hoechst 33342 staining (Invitrogen, USA), a DNA-specific dye, was used to detect morphological changes in nuclear morphology. Cowanol concentrations of 0, 10, 20 and 30 μM were applied to cells for 24 h. Next, 5 μg/mL Hoechst 33342 was added to all samples, and the results were observed using a fluorescence microscope (IX73; Olympus, Tokyo, Japan).

Statistical analysis

The results were analyzed and expressed as the mean ± SD of 3 independent experiments. One-way ANOVA and Dunnett's multiple-comparison test were used for the statistical analysis in GraphPad Prism version 5.0 (San Diego, USA), and p values of $*p < 0.05$, $**p < 0.01$ and $***p < 0.005$ were viewed as significant.

Results and discussion

To predict the potential efficacy of cowanol as an HDAC inhibitor, *in silico* docking analysis was performed. The docking pose of cowanol to each HDAC active site was analyzed, and the fitness score in kcal/mol value was obtained. Additionally, the selectivity and mode of cowanol binding to each HDAC isoform's active site were determined using the HDAC inhibitors TSA, SAHA, and belinostat as reference inhibitors. As shown in **Table 1**, cowanol revealed a strong affinity for binding to both HDAC class I and II and the value was practically in the same range as the reference HDACi. Cowanol also demonstrated a preference for class II over class I, with HDAC 4 and HDAC 7 yielding values of 82.06 and 78.86 kcal/mol, respectively. It might be said that cowanol, particularly as a class II HDAC inhibitor, has the potential to function as an HDAC inhibitor.

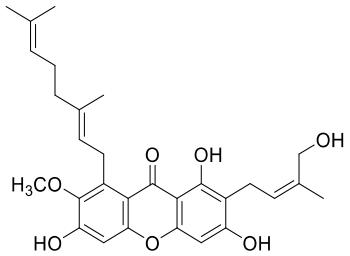

Cowanol

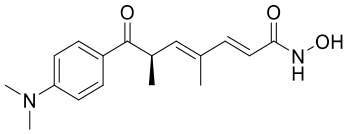

Trichostatin A (TSA)

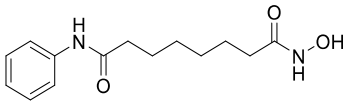

Vorinostat (SAHA)

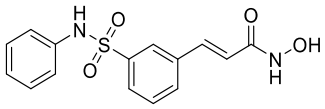

Belinostat

Figure 1 The chemical structure of cowanol extracted from the *Garcinia fusca* plant, preclinical HDACi drugs, trichostatin A (TSA), clinical HDACi, vorinostat (SAHA) and belinostat.

Table 1 The binding energy (kcal/mol) of all of these compounds.

Compounds	PubChem CID	Class I HDACs		Class II HDACs	
		HDAC2 (3MAX)	HDAC8 (1T64)	HDAC4 (4VQM)	HDAC7 (3C10)
TSA	444732	92.81	73.8	79.48	89.04
SAHA	5311	80.79	72.61	70.3	68.57
Belinostat	6918638	72.85	72.85	74.71	74.84
Cowanol	10480887	93.56	79.5	92.58	108.14

To further explore the potential function of cowanol, it was necessary to understand its method of binding and important interactions in the active sites of each HDAC. The active sites of each HDAC isoform, including class I (HDAC 2, HDAC 8) and class II (HDAC 4, HDAC 7), were then superimposed with cowanol and the reference inhibitors (**Figure 2**). As shown in **Figures 2(A)** and **2(B)**, the results indicated that cowanol and all inhibitors were oriented and had a similar binding pose in the active regions of HDAC 2 and HDAC 8. However, because of the bulky structure of the xanthone core and the long, narrow tube of the HDAC active sites, the interactions between cowanol and several important residues nearby to Zn^{2+} binding were loose. The findings suggested that because the class I isoforms have various ways of binding, cowanol may have lower enzymatic activity than HDAC inhibitors.

According to **Figures 2(C)** and **2(D)**, none of the ligands in HDAC class II displayed perfect overlap and aligned in the same direction. However, they continued to make it known to the zinc-binding group that they needed to chelate the Zn^{2+} ion's strong binding to the active sites of both HDAC 4 and HDAC 7. A rise in the hydrophobic interactions in the HDAC class II active sites, where the binding pocket and cavity are greater than in class I, may also be influenced by the long side chains and aromatic ring of cowanol. The collected information demonstrated that class II HDACs are specifically inhibited by cowanol.

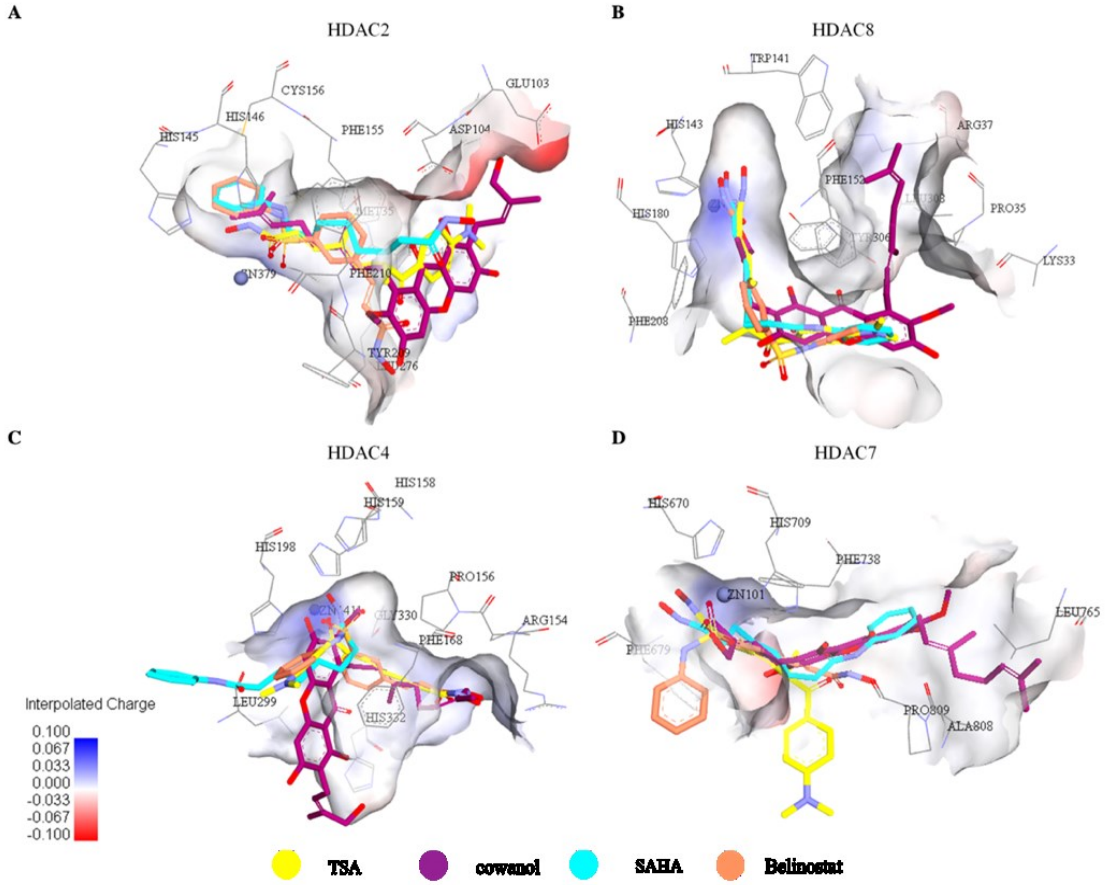

Figure 2 Superimposition of HDACi ligands TSA (yellow), SAHA (blue-green), belinostat (orange) and cowanol ligand (magenta) with a metal ion (Zn^{2+}) and key amino acid residues in the catalytic pocket site of HDAC enzymes (A) HDAC2, (B) HDAC8, (C) HDAC4 and (D) HDAC7 analyzed using the BIOVIA Discovery studio program.

Since HDACs are metalloenzymes that have Zn^{2+} ions as cofactors of HDACs, then the effective HDACi should bind with or chelate metal ion and key amino acid residues at the catalytic active site [30]. As demonstrated by known HDACis, TSA, SAHA and Belinostat, the predicted ligands-enzymes interaction showed that all HDACis fit into the catalytic pocket site of HDACs and bound with Zn^{2+} ions as well as key amino acid residues [27,30]. As shown in **Figures 3** and **4**, cowanol and reference inhibitors could bind similarly to each HDAC isoform's active site to create the chelated Zn^{2+} ion and key amino acid residues except for HDAC 2. The lack of ligand-metal complex interactions in HDAC 2 resulted in weaker binding affinity when compared to other isoforms. Cowanol, on the other hand, indicated a flexible chain as a geranyl group in the hydrophobic tunnel in HDAC 2, which has no interaction group for zinc binding, resulting in a reduction in the binding energy. Then, the hydroxyl group of cowanol formed hydrogen bonds with the residues Glu103, Asp104 and His183 in the active sites of HDAC 2, as can be clearly explained in **Figures 3(A)**, **3(C)** and **Table 2**. Moreover, the xanthone core generated hydrophobic interactions with Leu276 and Pro34 in the binding pocket of HDAC 2. Additionally, the cowanol geranyl and prenyl parts may interact with hydrophobic residues such as Phe210, Tyr308, Phe155, His33, His146 and His183 to form Pi-alkyl interactions.

The possible binding mode of cowanol on HDAC 8 is shown in **Figures 3(B)**, **3(D)** and **Table 2**. The hydroxyl group at the prenyl part chelated to the Zn^{2+} ion at the bottom of the HDAC 8 active site via His180, Asp178 and Asp267 residues. In addition to coordination with the zinc ion, an extra hydrogen bond was found between the hydroxyl group at the prenyl group and Asp178. The prenyl part occupied the hydrophobic tunnel of the active site with His143, Phe208, Phe152, and His180 residues. In addition, the hydroxyl group at the core ring could form hydrogen bonds to Tyr100 and Asp101. Then, the xanthone core represented as the cap group for HDACi, located at the entrance cavity, generated hydrophobic interactions with conserved residues Phe208 and Phe152. The geranyl side chain could bind to the Tyr306, Ile34, Pro35, Arg37 and Leu308 residues via hydrophobic interactions [31].

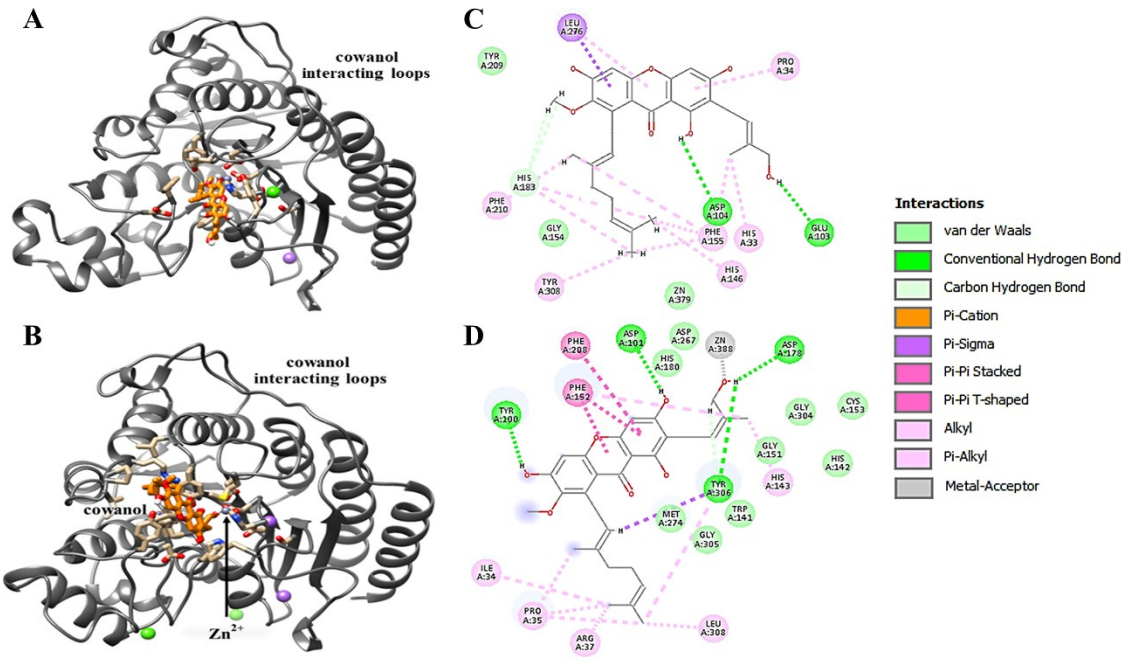

Figure 3 Molecular docking analysis of cowanol with human class I HDACs (HDAC 2 and 8). The analysis was predicted by using the GOLD docking program version 5.3.0. The HDAC 2 (A) and HDAC 8 (B) crystal structures (PDB ID: 3max and 1t64) were used to monitor cowanol interactions. The 2-dimensional (2D) interaction of cowanol along with the zinc ion and other amino acid residues of the catalytic center of HDAC 2 (C) and HDAC 8 (D) was demonstrated.

Table 2 Molecular interactions and interacting amino acid residues of the catalytic domain of HDAC class I (HDAC 2 and HDAC 8) with cowanol and positive HDACis.

	HDAC Class I							
	HDAC 2				**HDAC 8**			
Compound	**Cowanol**	**TSA**	**SAHA**	**Belinostat**	**Cowanol**	**TSA**	**SAHA**	**Belinostat**
Interaction **Conventional hydrogen**	ASP104, GLU103	HIS145, GLY154, TYR308	GLY154, ASP104	GLY154, TYR209, TYR308, LEU276	ASP101, ASP178, TYR100, TYR306	TYP306, ASP178, HIS142	TYP306, ASP178, HIS142	TYP306, GLY304, GLN263, ASP178, HIS142
Metal-acceptor	-	-	-	-	ZN388	-	-	-
Van der Waals	GLY154, TYR209, ZN379	GLU103, HIS146, GLY306, ZN379	HIS145, ZN379	LEU144, HIS145, GLY306, GLY277, ASP181, ZN379	ASP267, CYS153, GLY304, GLY305, GLY151, HIS142, HIS180, ASP101, TRP141, MET274	GLN263, GLY304, HIS143, HIS180, ASP101, MET274, ZN388	GLN263, GLY304, HIS143, HIS180, ASP101, ZN388	ASP267, GLY140, HIS143, ZN388

	HDAC Class I							
	HDAC 2				HDAC 8			
Compound	**Cowanol**	**TSA**	**SAHA**	**Belinostat**	**Cowanol**	**TSA**	**SAHA**	**Belinostat**
Pi-Pi T-shaped	-	PHE155	-	HIS183, PHE155	PHE152, PHE208	-	-	HIS180
Pi-sigma	LEU276	PHE210, HIS183	-	-	TYR306	PHE208	-	-
Pi-sulfur	-	-	CYS156	HIS146	-	-	-	MET274
Pi-alkyl	PRO34, PHE155, HIS146	PRO34, LEU276	LEU144, PHE155, PHE210, HIS146, HIS183	CYS156	PRO35, TYR306, PHE152, HIS143	TSN387, PHE152, PHE208	TSN387, PHE152, PHE208	-
Alkyl	PHE210, TYR308, H33	-	-	-	ILE34, ARG37, LEU308	-	-	-
Carbon hydrogen	HIS183	ASP104	-	-	-	TYR100	TYR100	GLY304

For HDAC 4 (**Figures 4(A)**, **4(C)** and **Table 3**), the core ring of cowanol showed Pi-Cation interactions with the residues located at the hydrophobic tunnel of the HDAC active sites, Arg37 and through Pi-alkyl interactions with Pro156, as shown in **Figures 4(A)** and **4(C)**. Then, the methoxy group of cowanol coordinated to the Zn^{2+} ion at the HDAC 4 active site via His198, Asp196 and Asp290 residues. In addition, a hydrogen bond occurred between the hydroxyl group of cowanol with Asp290 and His159. Interestingly, the methoxy group of cowanol formed a metal-acceptor interaction with the zinc ion, which was pivotal for the enzyme mechanism of HDAC 4, which was not present in other isoforms. Moreover, the conserved residues His159 and His198 were observed to form strong hydrogen bonds and hydrophobic interactions with cowanol at the bottom of the active site, respectively. The side chains of cowanol also occupied hydrophobic interactions with Phe168, Tyr170, Pro155, Pro156 and His198. Since cowanol posed methoxy and hydroxyl groups, which represented the zinc-binding group, fitting into the catalytic site of HDAC 4, we hypothesized that this feature together with the hydrogen bond between cowanol and the conserved residue His159 could be the reason for the potential role of selectivity toward HDAC 4.

For HDAC 7 (**Figure 4(B)**, **4(D)** and **Table 3**), cowanol pointed the prenylated group into the active site of HDAC 7; then, the hydroxyl group chelated with Zn^{2+} ions together with Asp801, Asp707, and His709. In addition, this side chain formed hydrophobic interactions with His709, Leu810, Phe679, Pro542, Arg547 and His843. His843 is a position pointing way from the active site of HDAC7 and is found exclusively in Class IIA HDACs to form interaction with Zn^{2+} ions [32]. The hydrogen bonds of cowanol were formed to Asp626 and Gly678, which are located at the bottom of the HDAC active site. Furthermore, the core ring of cowanol accommodated the Pi-Pi stacking interaction with Phe738.

Our results indicated that cowanol revealed a stronger affinity to class II (HDACs 4 and 7) than class I (HDACs 2 and 8) with scores of 82.06 and 78.86 kcal/mol, respectively. Moreover, our results of superimposed cowanol and reference inhibitors within the active site of each HDAC enzyme have supported that cowanol could be oriented and shared a similar binding pose in the active site, especially the interaction of HDAC class II with cofactor metal ion Zn^{2+} and key amino acid residues in a similar mode of binding to all HDAC inhibitors except in HDAC 2. Thus, these results confirmed that cowanol is a highly selective inhibitor of class II HDACs. In addition, the intermolecular attractions between cowanol and the catalytic site of each HDAC isoform also formed van der Waals interactions. In fact, van der Waals forces are the weakness of all interaction bonds between molecules, but the binding affinity can be increased when many van der Waals forces occur [33-35]. Taken together, all data from computational studies indicated that cowanol is a potential HDACi that can chelate zinc ions and bind specifically into the catalytic pocket sites of both HDAC class I and II when compared with positive HDAC inhibitors control as shown in Supplementary **Figure S(1)**.

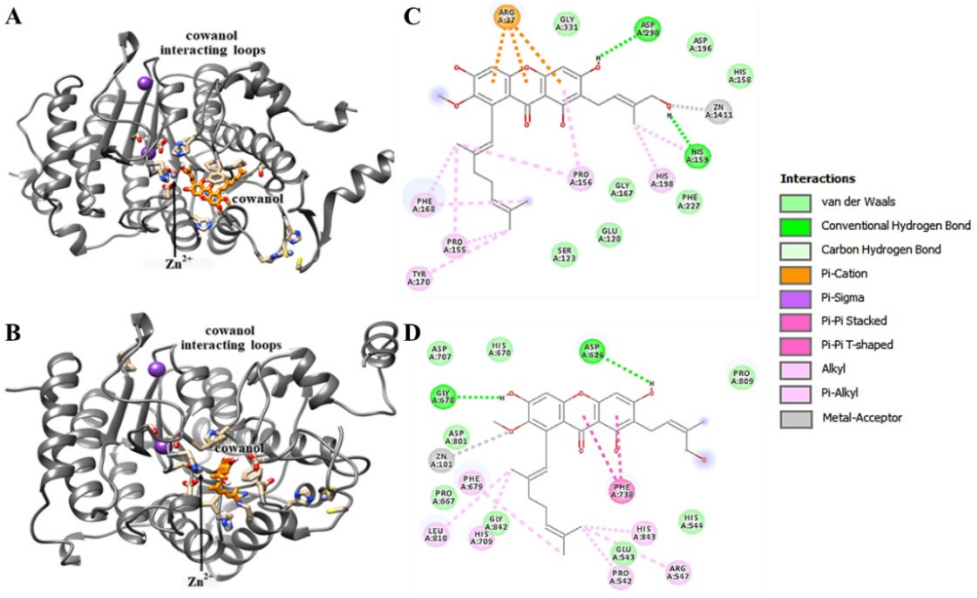

Figure 4 Molecular docking analysis was predicted by using the GOLD docking program version 5.3.0. (A) - (B) The human HDAC class II (HDACs 4 and 7) crystal structure (PDB ID: 4vqm and 3c10) was used to monitor cowanol interactions. (C) - (D) 2-dimensional (2D) interaction of cowanol along with the zinc ion and other amino acid residues of the catalytic center.

Table 3 Molecular interactions and interacting amino acid residues of the catalytic domain of HDAC class II (HDAC 4 and HDAC 7) with cowanol and positive HDACis.

	HDAC Class II							
	HDAC 4				**HDAC 7**			
Compound	**Cowanol**	**TSA**	**SAHA**	**Belinostat**	**Cowanol**	**TSA**	**SAHA**	**Belinostat**
Interaction **Conventional hydrogen**	HIS159, ASP290	ARG154	ASP196, HIS158	GLY167, ARG154	GLY678, ASP626	HIS669, ASP707	HIS669, HIS670, ASP707	PRO809
Metal-acceptor	ZN1411	ZN1411	ZN1411	-	ZN101	-	-	-
Van der Waals	GLY167, GLY331, ASP196, HIS158, PHE227, GLU120, SER123	HIS159	HIS159, HIS198, GLU329	ASP196, GLY331, ARG37, ZN1411	HIS544, HIS669, HIS670, PRO667, PRO806, ASP707, ASP801, ARG547, GLY678, PHE738, GLU543	HIS670, GLU840, HIS709, ZN101	PHE738, PRO542, PRO667, GLY678, HIS709, ZN101	HIS544, HIS669, HIS843, PRO667, ASP707, ASP801, ARG547, GLY678, ZN101
Pi-cation	ARG37	-	-	-	-	-	-	-
Pi-Pi T-shaped	-	HIS198	PHE168	HIS198	-	-	-	HIS709
Pi-sigma	-	PHE227	-	-	-	LEU810, PHE679, PHE738	-	-
Pi-sulfur	-	-	-	HIS158, HIS159	-	-	-	HIS670, PHE679
Pi-alkyl	PHE168, HIS159, PRO155, PRO156	PHE168, PHE277	PHE227	PRO156	PHE679, LEU810, HIS709	PRO542	PHE679	PRO542
Alkyl	TYR170, HIS198	-	-	-	HIS843, PRO542, AGR547	LEU810	-	-
Carbon hydrogen	-	-	-	ARG37	-	-	-	-

For drug-likeness prediction, the potential physical properties of cowanol and the known HDACi, TSA, SAHA and Belinostat were investigated by considering 6 physicochemical properties such as molecular weight (MW), the numbers of hydrogen bond donors (HBD), hydrogen bond acceptors (HBA), the numbers of rotatable bond (RB), polar surface area (PSA), and molinspiration lipophilicity (MLogP) using *in silico* SwissADME web tool [28]. Through radar image has been shown in Table 4, the predicted results revealed that cowanol demonstrated acceptable pharmacokinetics and drug-likeness properties following Lipinski's rule of 5 criteria: (i) MW ≤ 500 Da, (ii) HBD ≤ 5 and HBA ≤ 10, (iii) RB ≤ 10, (v) PSA ≤ 140 Å, (iv) MLogP ≤ 5 [36,37]. The prediction of bioavailability radar of cowanol and 3 known HDACis (**Figure 5**) suggested that all compounds are expected to be oral bioavailability (less toxic and good absorption), less polarity and flexibility. Therefore, the finding suggested that cowanol could likely be developed as a promising natural anticancer agent.

Table 4 Comparative physiochemical predicted Lipinski's rule of 5 for the phytochemical of cowanol, pre-clinical, and clinical drugs under study. MW, Molecular Weight; HBD, hydrogen bond donor; HBA, hydrogen bond acceptor; RB, number of rotatable bonds; PSA, polar surface area; MLogP, molinspiration Log partition coefficient.

Compound	Lipinski's Rule of Five						Drug-Likeness
	MW (≤500 Da)	HBD (≤5)	HBA (≤10)	RB (≤10)	PSA (≤140 Å)	MLogP (≤5)	
cowanol	494.58	4	7	9	120.36	2.33	Yes
TSA	302.37	2	3	7	69.64	2.01	Yes
SAHA	264.32	3	3	10	78.43	1.83	Yes
Belinostat	318.35	3	4	6	103.88	1.55	Yes

To confirm the HDACi effect *in vitro* of cowanol, an HDAC screening assay was performed. As depicted in **Table 5** and **Figure 6**, cowanol could inhibit the activity of human HDAC enzymes, which was consistent with the *in silico* docking analysis. However, the efficiency of cowanol was significantly lower than that of the standard SAHA because cowanol lacked the strong zinc-binding group, which is the key enzymatic activity of HDAC. Even though the binding energy of cowanol obtained was stronger than that of the standard inhibitors, it still lost some key interactions with some conserved residues for HDAC catalytic activity. In addition, docking studies were specifically analyzed in certain HDACs, while the HDAC inhibitor assay screened all HDACs in the cell lysate. In addition, SAHA functions as a pan-HDAC inhibitor. Therefore, our data may indicate that cowanol tends to inhibit some HDACs, especially HDAC 4 and may not act as a pan inhibitor.

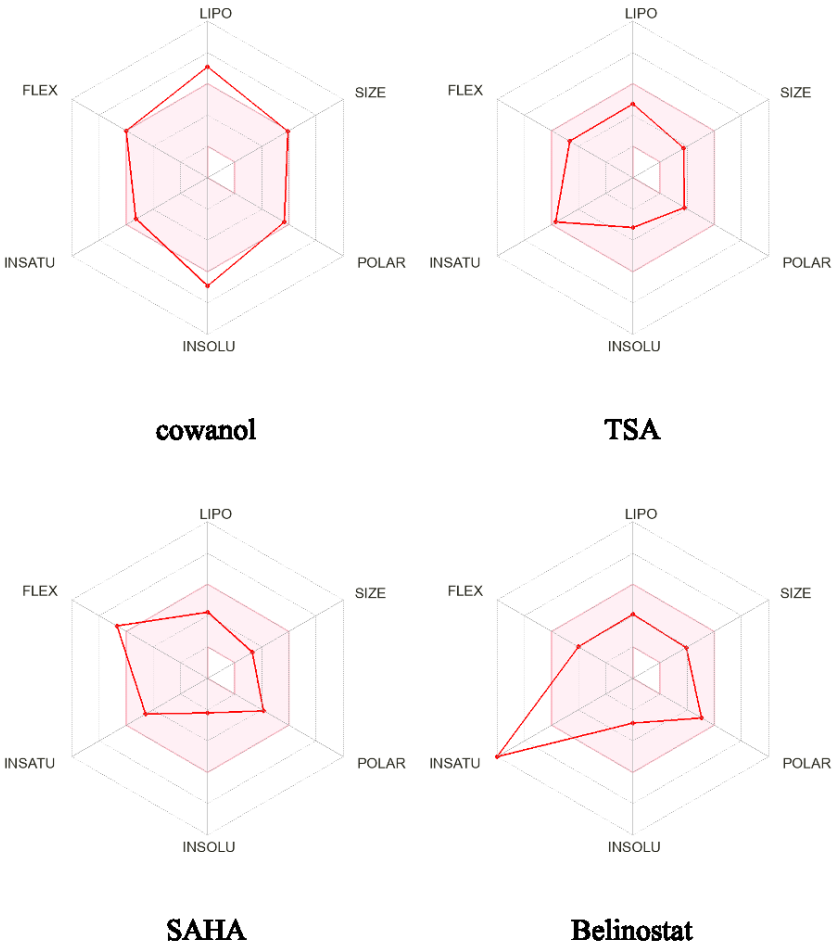

Figure 5 Schematic diagram of radar charts for prediction of oral bioavailability generated by the SwissADME web tool. This chart contains 6 axes for the 6 factors necessary for oral bioavailability; flexibility (FLEX), lipophilicity (LIPO), size (SIZE), polarity (POLAR), solubility (INSOLU) and saturation (INSATU), and the pink area in this chart illustrates the ideal ranges for predicted good oral bioavailability.

Table 5 The percentage of HDAC inhibition by cowanol. The clinical HDACi SAHA (10 µM) was used as a positive control, whereas DMSO was used as a negative control.

Cowanol concentration (µM)	HDAC inhibition (%)
0	0.00 ± 0.00
5	16.28 ± 1.50
25	23.75 ± 0.41
50	34.53 ± 0.51
100	46.71 ± 0.76
200	56.89 ± 1.89
SAHA	84.34 ± 1.19

*SAHA = clinical HDAC inhibitor (10 µM)

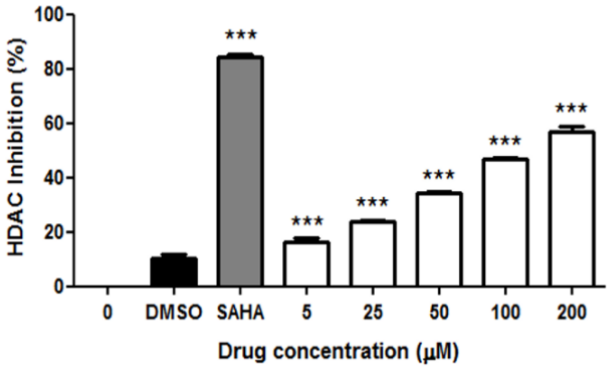

Figure 6 Cowanol treatment inhibits HDAC activity. Different concentrations of cowanol at 0, 5, 25, 50, 100 and 200 μM were incubated with Jurkat nuclear lysates, source of human HDAC enzymes, substrate, and developer for 10 - 20 min and subsequently detected by fluorescence microscopy. As a reference HDACi, SAHA was used, whereas DMSO was a negative control. Statistical analysis of cowanol-mediated HDAC inhibition was analyzed with one-way ANOVA Dunnett's multiple comparison test, ***$p < 0.001$, a significant difference compared to the control.

To further evaluate the anticancer effect of cowanol and the sequential mechanism of apoptotic cell death, Jurkat, PC-3 and A549 cells as well as Vero cells, representative of normal cells, were used as models. Cell viability was determined by MTT assay and the IC_{50} value is shown in **Table 6**. Our results indicated that cowanol had cytotoxic effect to all cancer cells tested but less effect to the representative of normal cells. The highest toxicity was clearly indicated in Jurkat cells with IC_{50} values of 24.77 ± 0.63, 20.33 ± 0.43 and 18.19 ± 0.44 μM at 24, 48 and 72 h, respectively, whereas normal Vero cells showed lower activity (IC_{50} > 100 μM). To compare the cytotoxicity of cowanol with standard drug, SAHA was selected to perform MTT assay. As shown in **Figure 7**, the cytotoxic effect of cowanol has higher potency than SAHA, supporting the role of anticancer agent. Thus, this data suggested that the consequences of cowanol acting highly potent cytotoxic activities against cancer cells but nontoxic to normal cells.

Table 6 IC_{50} of cowanol against Jurkat, A549, PC-3, and Vero cells after 24, 48 and 72 h of incubation.

Cancer cells	Cowanol IC_{50} value (μM)		
	24 h	48 h	72 h
Jurkat	24.77 ± 0.63	20.33 ± 0.43	18.19 ± 0.44
PC-3	88.67 ± 1.82	75.45 ± 0.78	46.01 ± 0.76
A549	96.83 ± 0.72	69.43 ± 1.44	52.74 ± 0.25
Vero	>100	>100	>100

Moreover, the cytotoxic doses of cowanol are also correlated well to other xanthones. For example, α-, β- and γ-mangostin could inhibit cell growth via caspase-3 activation at a low dose of 10 μM, whereas mangostinone, garcinone E and 2-isoprenyl-1,4-dihydroxy-3-methoxyxanthone exhibited IC_{50} values of 19, 15 and 23.6 μM in HL60 cells [38]. Additionally, the cytotoxic effects on leukemic cells of β-mangostin, which was isolated from *Cratoxylum arborescent*, could inhibit cell growth at a concentration of 58 μM and induce the apoptosis pathway via ROS with downregulation of the HSP70 gene associated with G0/G1 cell cycle arrest in leukemia cells (HL-60) [39]. From the MTT results, the data also showed that cowanol had low toxicity effect on normal Vero cells with IC_{50} values higher than 100 μM. This data correlated well with our previous study, which reported that cowaxanthone, pure extracted compound from *Garcinia fusca* had less toxicity to Vero cells with IC_{50} values of 110.40 ± 6.13 μM [20]. These findings indicated the advantageous properties of cowanol for cancer treatment with high safety potency. Therefore, we further investigated the mode of cell death induced by cowanol and selected Jurkat cells as a model.

For apoptosis induction, Jurkat cells were exposed to cowanol and stained with Hoechst 33342, a fluorescence DNA-specific dye, for 24 h. Cowanol promoted changes in nuclear morphology and the formation of apoptotic bodies, which were clearly observed from 10 µM, as shown in **Figure 8**. Such morphological changes are also considered as morphological hallmarks of apoptosis, while fragmentation of DNA or apoptotic bodies, protein cleavage, and protein cross-linking as biochemical hallmarks of apoptosis [40]. These results provide strong evidence that cowanol could induce Jurkat leukemic T cells to undergo apoptosis. Our findings were in agreement with those of other HDACi substances, such as kaempferol [41], resveratrol [42], and the isoquinoline alkaloid berberine [43], which have been shown to trigger apoptosis in cancer cells. Additionally, many xanthone compounds have the potential to trigger the apoptosis pathway. Zhongyan *et al.* (2020) [44] showed that isojacareubin could inhibit cell proliferation and induce apoptosis via PARP, PI3K/AKT/mTOR, and ERK/MAPK pathways in the ovarian cancer HEY cells [44]. In human lung cancer (A549) cells, they also found that cratoxylumxanthone C could increase ROS production and G0/G1 cell cycle arrest through changes the expression levels of apoptosis-related proteins. Additionally, this compound also inhibits cell proliferation and metastasis by down-regulating STAT3, FAK, and MMP-2 [45]. Moreover, another dietary xanthone α-mangostin (α-MGT), could induce cell cycle arrest and apoptosis in hepatocellular carcinoma (HCC) cells by inducing the cleavage of poly ADP-ribose polymerase (PARP), a well-known biomarker of apoptosis [46].

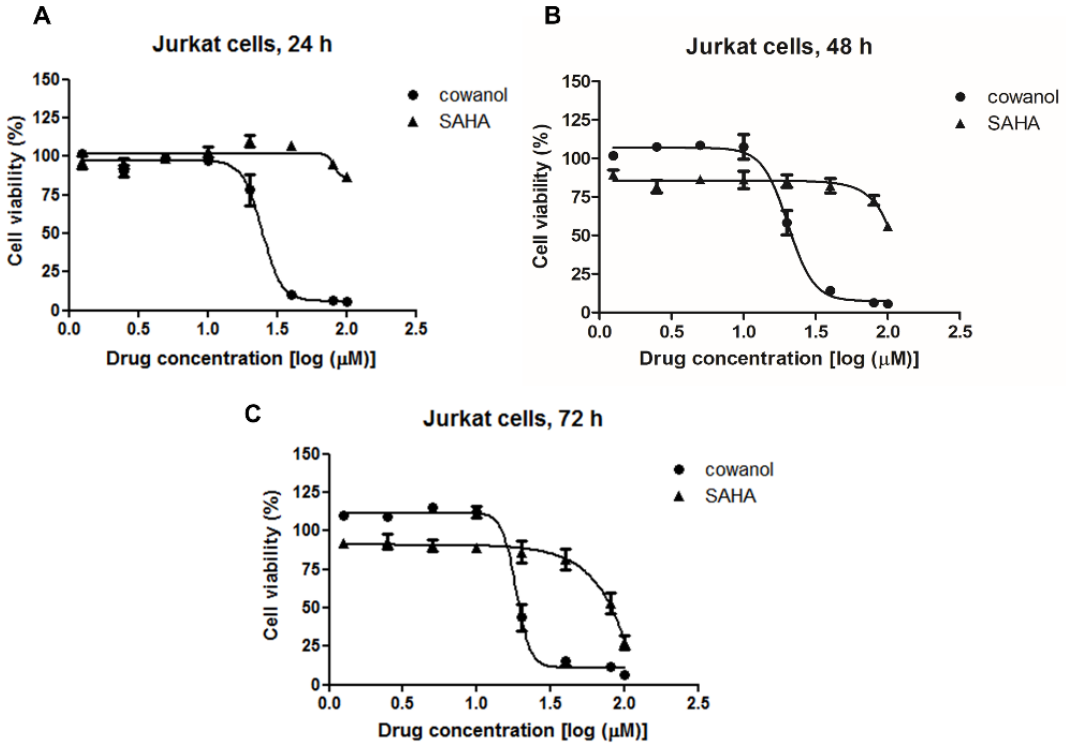

Figure 7 Cowanol and SAHA exhibited an inhibitory effect on the cell viability of Jurkat cells. Cells were treated with various concentrations of cowanol at 0 - 100 µM (0.5 % DMSO served as a negative control) for 24, 48 and 72 h (A) - (C). The results are presented as the percentage reduction of cell proliferation, which was directly proportional to formazan. Data are represented as the mean ± SD of 3 independent experiments performed in triplicate (n = 3). *$p < 0.05$, *** $p < 0.001$, versus the untreated cells.

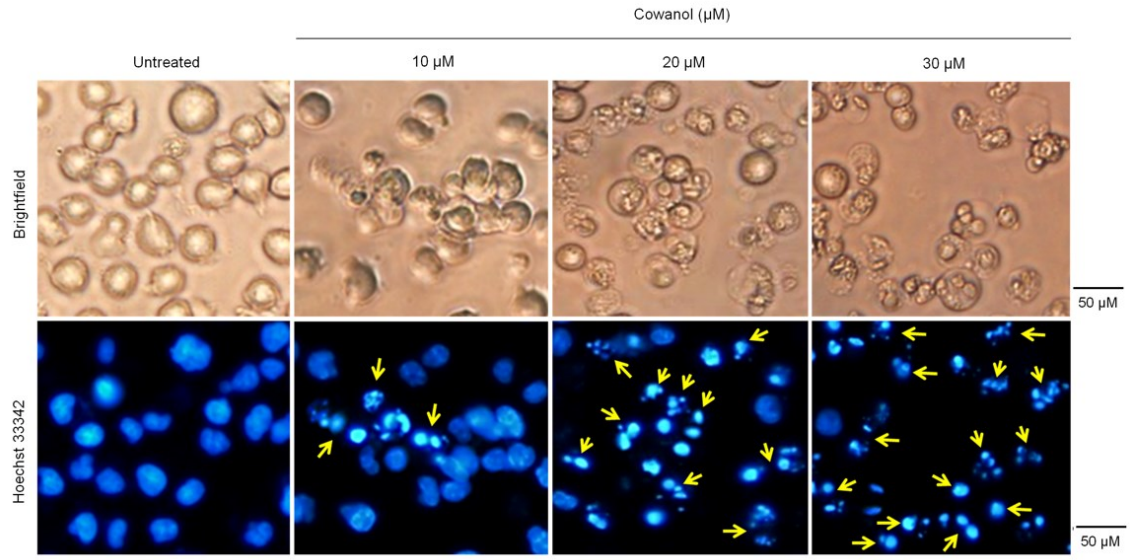

Figure 8 Cowanol induced DNA fragmentation in Jurkat cells. Cells were treated with 0.5 % DMSO (0 μM) and cowanol at 10, 20 and 30 μM for 24 h before being stained with Hoechst 33342 at a final concentration of 5 μg/mL. The nuclear and apoptotic morphology was determined by condensation, and fragmented nuclei were observed with an Olympus Reflected Fluorescence System microscope at 50x magnification. Bright-field (upper) and fluorescent dye Hoechst 33342 (lower).

Conclusions

These results showed a new potency of cowanol cytotoxicity to cancer cell proliferation, which distinctly differs from normal cells. Furthermore, according to our findings, cowanol administration inhibits the activity of HDACs. This suppression was most likely caused by the increased apoptotic impact, which might be used as a therapeutic target for Jurkat leukemic T cells. Additionally, the molecular docking analysis was performed to ensure the outstanding anticancer activities of the investigated compound by declaring their binding interactions with the Zn^{2+} cofactor and the catalytic-binding residues of HDACs. Similarly, the SwissADME online web software predicted that cowanol possessed acceptable physicochemical, drug-likeness properties, and oral bioavailability were obtained. Therefore, all of these findings point to cowanol as an interesting substance that merits further research and development as an anticancer drug.

Acknowledgments

The authors would like to thank the Innovative Learning Center (ILC) for its research support and the Strategic Wisdom and Research Institute, Department of Biochemistry, Faculty of Medicine, Srinakharinwirot University, Bangkok, Thailand. We also thank the Center of Excellence for Innovation in Chemistry (PERCH-CIC), the Ministry of Higher Education, Science, Research and Innovation, and the Department of Chemistry, Faculty of Science, Srinakharinwirot University, for their support.

References

[1] LJ Castro-Munoz, EV Ulloa, C Sahlgren, M Lizano, EDL Cruz-Hernandez and A Contreras-Paredes. Modulating epigenetic modifications for cancer therapy (Review). *Oncol. Rep.* 2023; **49**, 59.
[2] G Li, Y Tian and WG Zhu. The roles of histone deacetylases and their inhibitors in cancer therapy. *Front. Cell Dev. Biol.* 2020; **8**, 576946.
[3] Z Rana, JDA Tyndall, M Hanif, CG Hartinger and RJ Rosengren. Cytostatic action of novel histone deacetylase inhibitors in androgen receptor-null prostate cancer cells. *Pharmaceuticals* 2021; **14**, 103.
[4] H Mamdani and SI Jalal. Histone deacetylase inhibition in non-small cell lung cancer: Hype or hope? *Front. Cell Dev. Biol.* 2020; **8**, 582370.
[5] T Liang, F Wang, R M Elhassan, Y Cheng, X Tang, W Chen, H Fang and X Hou. Targeting histone deacetylases for cancer therapy: Trends and challenges. *Acta Pharm. Sin. B* 2023; **13**, 2425-63.

[6] N Garmpis, C Damaskos, D Dimitroulis, G Kouraklis, A Garmpi, P Sarantis, E Koustas, A Patsouras, I Psilopatis, EA Antoniou, MV Karamouzis, K Kontzoglou, A Nonni and A Nonni. Clinical significance of the histone deacetylase 2 (HDAC-2) expression in human breast cancer. *J. Pers. Med.* 2022; **12,** 1672.

[7] H Jo, K Shim, HU Kim, HS Jung and D Jeoung. HDAC2 as a target for developing anti-cancer drugs. *Comput. Struct. Biotechnol. J.* 2023; **21**, 2048-57.

[8] JY Kim, H Cho, J Yoo, GW Kim, YH Jeon, SW Lee and SH Kwon. HDAC8 deacetylates HIF-1alpha and enhances its protein stability to promote tumor growth and migration in melanoma. *Cancers* 2023; **15,** 1123.

[9] JY Kim, H Cho, J Yoo, GW Kim, YH Jeon, SW Lee and SH Kwon. Pathological role of HDAC8: Cancer and beyond. *Cells* 2022; **11**, 3161.

[10] M Zhou, M Yuan, M Zhang, C Lei, O Aras, X Zhang and F An. Combining histone deacetylase inhibitors (HDACis) with other therapies for cancer therapy. *Eur. J. Med. Chem.* 2021; **226**, 113825.

[11] S Kaennakam, E R Sukandar, P Phasuthan, J Yahuafai, P Onsrisawat, F Mulya, V Parasuk, P Phuwapraisirisan and S Tip-Pyang. Garcowacinols A-J, cytotoxic polyprenylated benzoylphloroglucinol derivatives from the twigs of Garcinia cowa. *Phytochemistry* 2023; **209**, 113622.

[12] IP Dewi, FS Wahyuni, Y Aldi, NH Ismail and Dachriyanus. *In vitro* immunomodulatory activity study of *Garcinia cowa* Roxb. fraction. *J. Compl. Integr. Med.* 2023; **20**, 365-71.

[13] A Chouni and S Paul. A comprehensive review of the phytochemical and pharmacological potential of an evergreen plant *Garcinia cowa*. *Chem. Biodivers.* 2023; **20**, e202200910.

[14] J Tauchen, A Frankova, A Manourova, I Valterova, B Lojka and O Leuner. *Garcinia kola*: A critical review on chemistry and pharmacology of an important West African medicinal plant. *Phytochem. Rev.* 2023; **22**, 1305-51.

[15] PFS Etet, MA Hamza, A El-Tahir, L Vecchio, SY Osman, GMH Satti, MHA Ismail, M Farahna, AK Njamnshi and A Adem. An eluate of the medicinal plant garcinia kola displays strong antidiabetic and neuroprotective properties in streptozotocin-induced diabetic mice. *Evid. Based Compl. Alternative Med.* 2022; **2022**, 8708961.

[16] SD Vita, M Masullo, S Grambone, PB Bescós, S Piacente and G Bifulco. Demethylcalabaxanthone from garcinia mangostana exerts antioxidant effects through the activation of the Nrf2 pathway as assessed via molecular docking and biological evaluation. *Antioxidants* 2023; **12**, 1980.

[17] P Patil, M Agrawal, S Almelkar, M K Jeengar, A More, K Alagarasu, NV Kumar, PS Mainkar, D Parashar and S Cherian. *In vitro* and *in vivo* studies reveal alpha-mangostin, a xanthonoid from Garcinia mangostana, as a promising natural antiviral compound against chikungunya virus. *Virol. J.* 2021; **18**, 47.

[18] A Saenkham, A Jaratrungtawee, Y Siriwattanasathien, P Boonsri, K Chainok, A Suksamrarn, M Namsa-Aid, P Pattanaprateeb and S Suksamrarn. Highly potent cholinesterase inhibition of geranylated xanthones from Garcinia fusca and molecular docking studies. *Fitoterapia* 2020; **146**, 104637.

[19] S Punpai, A Saenkham, F Jarintanan, S Jongrungruangchok, K Choowongkomon, S Suksamrarn and W Tanechpongtamb. HDAC inhibitor cowanin extracted from G. fusca induces apoptosis and autophagy via inhibition of the PI3K/Akt/mTOR pathways in Jurkat cells. *Biomed. Pharmacother.* 2022; **147**, 112577.

[20] S Punpai, A Saenkham, K Choowongkomon, S Suksamrarn and W Tanechpongtamb. *In silico* and *in vitro* analysis of the role of cowaxanthone as a histone deacetylase inhibitor and apoptosis inducer in human leukemic T-cells. *J. Curr. Sci. Tech.* 2020; **10**, 183-94.

[21] BLSDE Santo, LF Santana, WHK Junior, FDOD Araújo, D Bogo, KDC Freitas, RDCA Guimarães, PA Hiane, A Pott, WFDO Filiú, MA Asato, PDO Figueiredo and PRHDO Bastos. Medicinal potential of garcinia species and their compounds. *Molecules* 2020; **25**, 4513.

[22] VA Tran, TTT Vo, MNT Nguyen, ND Dat, VD Doan, TQ Nguyen, QH Vu, VT Le and TD Tong. Novel α-mangostin derivatives from mangosteen (Garcinia mangostana L.) peel extract with antioxidant and anticancer potential. *J. Chem.* 2021; **2021**, 9985604.

[23] LD Ha, PE Hansen, O Vang, F Duus, HD Pham and LH Nguyen. Cytotoxic geranylated xanthones and O-alkylated derivatives of alpha-mangostin. *Chem. Pharm. Bull.* 2009; **57**, 830-4.

[24] EF Bulbul, J Melesina, HS Ibrahim, M Abdelsalam, A Vecchio, D Robaa, M Zessin, M Schutkowski and W Sippl. Docking, binding free energy calculations and *in vitro* characterization of pyrazine

linked 2-aminobenzamides as novel class i histone deacetylase (HDAC) inhibitors. *Molecules* 2022; **27**, 2526.
[25] A Maruca, R Rocca, R Catalano, F Mesiti, G Costa, D Lanzillotta, A Salatino, F Ortuso, F Trapasso, S Alcaro and A Artese. Natural products extracted from fungal species as new potential anti-cancer drugs: A structure-based drug repurposing approach targeting HDAC7. *Molecules* 2020; **25**, 5524.
[26] N Jansch, KL Lang and FJ Meyer-Almes. Methionine 274 is not the determining factor for selective inhibition of histone deacetylase 8 (HDAC8) by L-shaped inhibitors. *Int. J. Mol. Sci.* 2022; **23**, 11775.
[27] B Scafuri, P Bontempo, L Altucci, LD Masi and A Facchiano. Molecular docking simulations on histone deacetylases (HDAC)-1 and -2 to investigate the flavone binding. *Biomedicines* 2020; **8**, 568.
[28] RD Hernandez, FAF Genio, JR Casanova, MT Conato and MC Paderes. Antiproliferative activities and swissADME predictions of physicochemical properties of carbonyl group-modified rotenone analogues. *ChemistryOpen* 2023; **13**, e202300087.
[29] CPMD Silva, GMD Neves, GLV Poser, VL Eifler-Lima and SMK Rates. *In silico* prediction of ADMET/Drug-likeness properties of bioactive phloroglucinols from *hypericum* genus. *Med. Chem.* 2023; **19**, 1002-17.
[30] A Drakontaeidi and E Pontiki. A review on molecular docking on HDAC isoforms: Novel tool for designing selective inhibitors. *Pharmaceuticals* 2023; **16**, 1639.
[31] AI Uba and G Zengin. Phenolic compounds as histone deacetylase inhibitors: Binding propensity and interaction insights from molecular docking and dynamics simulations. *Amino Acids.* 2023; **55**, 579-93.
[32] A Schuetz, J Min, A Allali-Hassani, M Schapira, M Shuen, P Loppnau, R Mazitschek, NP Kwiatkowski, TA Lewis, RL Maglathin, TH McLean, A Bochkarev, AN Plotnikov, M Vedadi and CH Arrowsmith. Human HDAC7 harbors a class IIa histone deacetylase-specific zinc binding motif and cryptic deacetylase activity. *J. Biol. Chem.* 2008; **283**, 11355-63.
[33] F Desantis, M Miotto, LD Rienzo, E Milanetti and G Ruocco. Spatial organization of hydrophobic and charged residues affects protein thermal stability and binding affinity. *Sci. Rep.* 2022; **12**, 12087.
[34] Y Kawasaki, EE Chufan, V Lafont, K Hidaka, Y Kiso, LM Amzel and E Freire. How much binding affinity can be gained by filling a cavity? *Chem. Biol. Drug Des.* 2010; **75**, 143-51.
[35] S Cho, CP Swaminathan, J Yang, MC Kerzic, R Guan, MC Kieke, DM Kranz, RA Mariuzza and EJ Sundberg. Structural basis of affinity maturation and intramolecular cooperativity in a protein-protein interaction. *Structure* 2005; **13**, 1775-87.
[36] R Leechaisit, P Mahalapbutr, P Boonsri, K Karnchanapandh, T Rungrotmongkol, V Prachayasittikul, S Prachayasittikul, S Ruchirawat, V Prachayasittikul and R Pingaew. Discovery of novel naphthoquinone-chalcone hybrids as potent FGFR1 tyrosine kinase inhibitors: Synthesis, biological evaluation, and molecular modeling. *ACS Omega* 2023; **8**, 32593-605.
[37] P Mahalapbutr, R Leechaisit, A Thongnum, D Todsaporn, V Prachayasittikul, T Rungrotmongkol, S Prachayasittikul, S Ruchirawat and V Prachayasittikul and R Pingaew. Discovery of anilino-1,4-naphthoquinones as potent EGFR tyrosine kinase inhibitors: Synthesis, biological evaluation, and comprehensive molecular modeling. *ACS Omega* 2022; **7**, 17881-93.
[38] K Matsumoto, Y Akao, E Kobayashi, K Ohguchi, T Ito, T Tanaka, M Iinuma and Y Nozawa. Induction of apoptosis by xanthones from mangosteen in human leukemia cell lines. *J. Nat. Prod.* 2003; **66**, 1124-7.
[39] FAA Omer, NBM Hashim, MY Ibrahim, F Dehghan, M Yahayu, H Karimian, . . ., S Mohan. Beta-mangostin from Cratoxylum arborescens activates the intrinsic apoptosis pathway through reactive oxygen species with downregulation of the HSP70 gene in the HL60 cells associated with a G0/G1 cell-cycle arrest. *Tumor Biol.* 2017; **39**, 1010428317731451.
[40] K Matsumoto, Y Akao, H Yi, K Ohguchi, T Ito, T Tanaka, E Kobayashi, M Iinuma and Y Nozawa. Preferential target is mitochondria in alpha-mangostin-induced apoptosis in human leukemia HL60 cells. *Bioorg. Med. Chem.* 2004; **12**, 5799-806.
[41] A Berger, S Venturelli, M Kallnischkies, A Bocker, C Busch, T Weiland, S Noor, C Leischner, TS Weiss, UM Lauer, SC Bischoff and M Bitzer. Kaempferol, a new nutrition-derived pan-inhibitor of human histone deacetylases. *J. Nutr. Biochem.* 2013; **24**, 977-85.
[42] S Venturelli, A Berger, A Bocker, C Busch, T Weiland, S Noor, C Leischner, S Schleicher, M Mayer, TS Weiss, SC Bischoff, UM Lauer and M Bitzer. Resveratrol as a pan-HDAC inhibitor alters the acetylation status of histone [corrected] proteins in human-derived hepatoblastoma cells. *PLoS One.* 2013; **8**, e73097.
[43] A Kalaiarasi, C Anusha, R Sankar, S Rajasekaran, J John Marshal, K Muthusamy and V Ravikumar. Plant isoquinoline alkaloid berberine exhibits chromatin remodeling by modulation of histone

deacetylase to induce growth arrest and apoptosis in the A549 cell line. *J. Agric. Food Chem.* 2016; **64**, 9542-50.

[44] Z Tang, L Lu and Z Xia. Anti-tumor xanthones from garcinia nujiangensis suppress proliferation, and induce apoptosis via PARP, PI3K/AKT/mTOR, and MAPK/ERK signaling pathways in human ovarian cancers cells. *Drug Des. Devel. Ther.* 2020; **14**, 3965-76.

[45] Y Li, H Wang, W Liu, J Hou, J Xu, Y Guo and P Hu. Cratoxylumxanthone C, a natural xanthone, inhibits lung cancer proliferation and metastasis by regulating STAT3 and FAK signal pathways. *Front. Pharmacol.* 2022; **13**, 920422.

[46] H Zhang, YP Tan, L Zhao, L Wang, NJ Fu, SP Zheng and XF Shen. Anticancer activity of dietary xanthone alpha-mangostin against hepatocellular carcinoma by inhibition of STAT3 signaling via stabilization of SHP1. *Cell Death Dis.* 2020; **11**, 63.

Supplementary

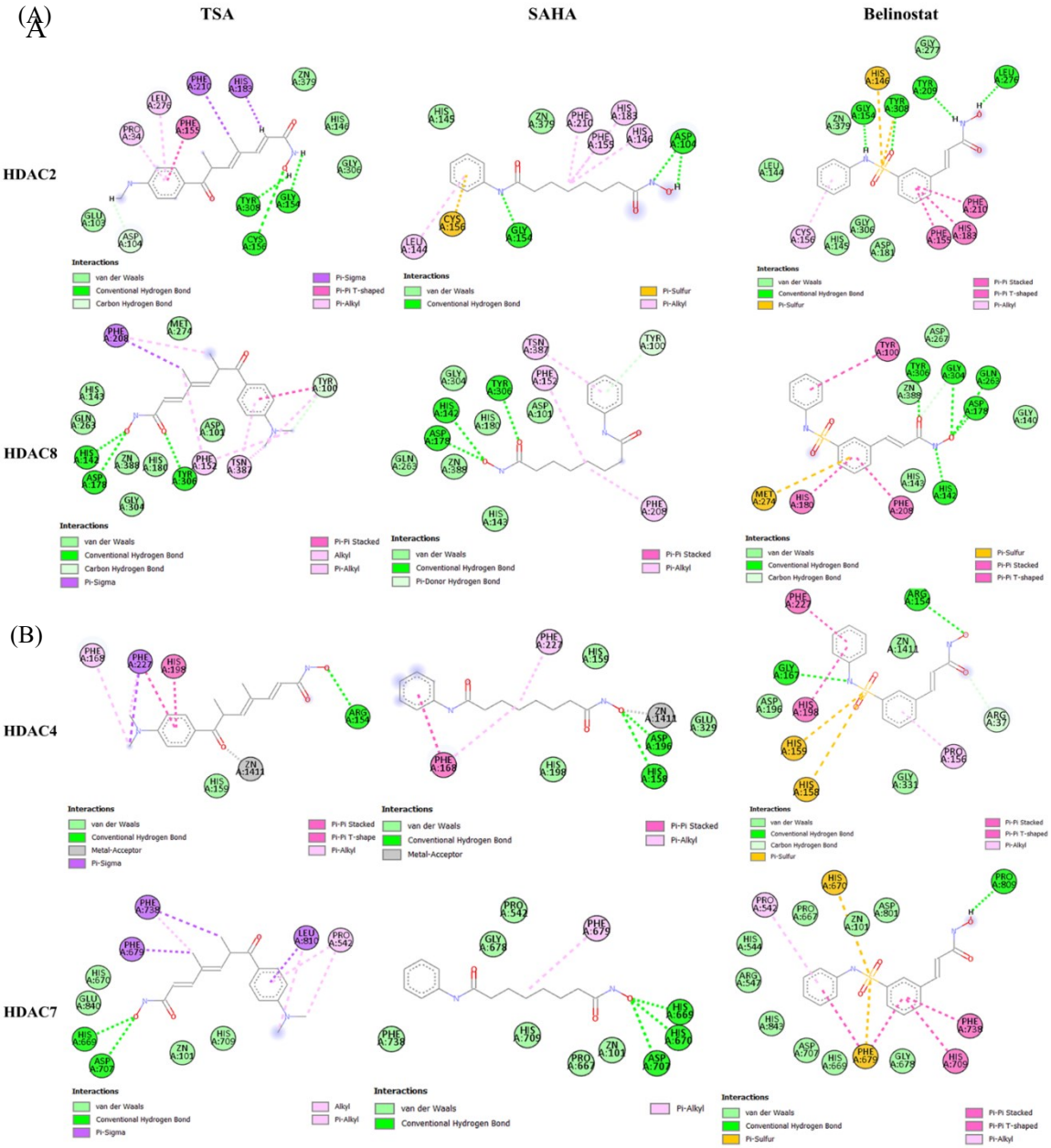

Figure S1 A two-dimensional (2D) depiction of the *in silico* docking illustrates the potential inhibitory effect of HDACis, TSA, SAHA, and Belinostat against human HDAC class I (HDAC2 and 8) and class II (HDAC4 and 7). The results of the 2D structure of the *in silico* docking analysis of all positive HDACis are predicted to interact with the zinc ion and key amino acid residues at the catalytic center (A-B).